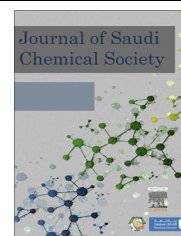




King Saud University

Journal of Saudi Chemical Society

[www.ksu.edu.sa](http://www.ksu.edu.sa)  
[www.sciencedirect.com](http://www.sciencedirect.com)


## ORIGINAL ARTICLE

# Corrosion inhibition of mild steel by highly stable polydentate schiff base derived from 1,3-propanediamine in aqueous acidic solution



Noura H. Alharthi<sup>a</sup>, Mohammed A. El-Hashemy<sup>a,b,\*</sup>, Wassila M. Derafa<sup>a,c</sup>, Ibrahim O. Althobaiti<sup>d</sup>, Hamud A. Altaleb<sup>e</sup>

<sup>a</sup> Department of Chemistry, College of Science, Jouf University, PO Box 2014, Sakaka, Saudi Arabia

<sup>b</sup> Air Pollution Research Department, Environmental and Climate Change Research Institute, National Research Centre, Dokki, Giza 12622, Egypt

<sup>c</sup> Laboratory of Electrochemistry, Molecular Engineering and Redox Catalysis, Department of Process Engineering, Faculty of Technology, University of Ferhat Abbas, Setif 19000, Algria

<sup>d</sup> Department of Chemistry, College of Science and Arts, Jouf University, Saudi Arabia

<sup>e</sup> Department of Chemistry, Faculty of Science, Islamic University of Madinah, PO Box 42351, Al-Madinah Al-Munawwarah, Saudi Arabia

Received 22 March 2022; revised 21 May 2022; accepted 29 May 2022

Available online 09 June 2022

## KEYWORDS

Schiff base;  
Corrosion inhibitor;  
Mild steel;  
SEM/EDX;  
FTIR;  
AFM;  
Adsorption isotherm

**Abstract** Recently, the hydrolysis of Schiff bases under experimental conditions gives suspicion for their corrosion inhibition performance. The current study employs a stable Schiff base namely, 2,2'-{propane-1,3-diylbis[azanylylidene (*E*) methanylylidene]}bis(6-methoxyphenol) (LPD) as corrosion inhibitor for mild steel (MS) in 1 M HCl solution. The presence of the characteristic peak of the imine group in UV-visible spectra was taken as an indicator for LPD stability in acidic media. The inhibition action was examined using electrochemical techniques including potentiodynamic polarization (PDP) and electrochemical impedance spectroscopy (EIS) besides gravimetric measurement. The inhibition efficiency reached 95.93 % for 0.75 mM LPD after 24 h of immersion at 25 °C. This high efficiency is owing to the presence of the characteristic imine group and other heteroatoms and  $\pi$ -electrons of the aromatic benzene rings. The mechanism of inhibition depends on adsorption phenomena on mild steel surface which obeys Langmuir isotherm model. The calculated values of adsorption equilibrium constant ( $K_{ads}$ ), adsorption free energy  $\Delta G_{ads}$ , adsorption enthalpy  $\Delta H_{ads}$  and adsorption entropy  $\Delta S_{ads}$  indicated spontaneous exothermic adsorption process of both physical and chemical nature. By rising temperature, the inhibition efficiency of LPD was decreased. The calculated activation energy was increased as the concentration of LPD increased. LPD was

\* Corresponding author.

Peer review under responsibility of King Saud University.



<https://doi.org/10.1016/j.jscs.2022.101501>

1319-6103 © 2022 The Author(s). Published by Elsevier B.V. on behalf of King Saud University.

This is an open access article under the CC BY-NC-ND license (<http://creativecommons.org/licenses/by-nc-nd/4.0/>).

considered as a mixed-type inhibitor as indicated from PDP measurements. The obtained surface morphology and composition analysis using SEM/EDS, AFM and FTIR techniques ensures the high efficiency of LPD as corrosion inhibitor.

© 2022 The Author(s). Published by Elsevier B.V. on behalf of King Saud University. This is an open access article under the CC BY-NC-ND license (<http://creativecommons.org/licenses/by-nc-nd/4.0/>).

## 1. Introduction

Mild steel (MS) corrosion has been the topic of many studies due to its numerous engineering applications. It is used in manufacturing of structural forms and sheets that are employed in plants, buildings, pipelines, and bridges, as well as some vehicle components[1]. On the other hand, MS is made of steel derived from pig iron, which is cheap to manufacture and widely accessible. It offers outstanding ductility and toughness, as well as excellent machinability and weldability, allowing it to be used in a variety of engineering fields[2]. It is necessary to consider the corrosion that engulfs MS to effectively employ it in various engineering applications.

Schiff bases (SB) are subclasses of imines that have the general structure ( $R^1R^2C = NR$ ). As a synonym for azomethine, the phrase is frequently used. Hugo Schiff, an Italian chemist, was named after these molecules[3].

Schiff bases are important in chemistry, notably in the development of SB complexes. They produce transition metals complexes having antiviral, antibacterial, and anticancer. SB and their metal complexes are known for their catalytic properties for various synthetic reactions. They are utilized as versatile instruments in a variety of utilities, such as fluorescent turn-on/turn-off sensors for the measurement of a variety of analytes [4].

According to the literature, nitrogen-based organic inhibitors work well in terms of corrosion prevention. Schiff base compounds are the most often employed among them. They have an interesting utility as corrosion inhibitors, this is due to their ability to establish a protective film on the metal surface. The structure of applied SB, type of the destructive medium as well as kind of interaction between the p-orbitals of these investigated compounds and the orbitals of the metal, influence the inhibitory effectiveness and mode of action of SB. The use of SB as corrosion inhibitors is based on the fact that they are easy to manufacture from commercially available chemicals with cheap cost, have minimal toxicity as it can be used in drug industry[5], and are ecofriendly compounds if prepared from safe compounds as sugars[6]. Furthermore, the presence of  $-C=N-$  and other donor substituents in SB allows it to easily adhere to metal surfaces and operate as an effective corrosion inhibitor for both ferrous and non-ferrous metals[7].

The performance of SB in aqueous solution in terms of corrosion inhibitor is well-documented. For the years 1979 to 2018, the Scopus database contains around 400 papers on the corrosion inhibition behavior of SB compounds mostly conducted in HCl and  $H_2SO_4$  solutions [8–11]. P.Rugmini Ammal et al. [51] studied the efficacy of 4-(4-hydroxy-3-methoxy benzylidene amino)-4-H-1,2,4-triazole-3,5-dimethanol as SB corrosion inhibitor for MS in 0.5 M HCl using gravimetric measurements and electro analytical procedures. Prajila et al. [12] investigated the inhibition properties of three SBs namely, (4-(4-methoxybenzylideneamino)-4H-1,2,4-triazole-3,5-diyldimethanol, (4-(3,4-dimethoxybenzylidene amino)-4H-1,2,4-triazole-3,5-diyldimethanol, and (4-(4-hydroxybenzylideneamino)-4H-1,2,4-triazole-3,5-diyldimethanol for MS corrosion in hydrochloric acid that have been investigated through weight loss, electrochemical, spectroscopic and computational analysis. According to the obtained results, these compounds were successful inhibitors for MS corrosion in HCl solution. Manilal Murmu et al. [13] synthesized a pair of SBs, namely, 4-(4-(4-(Pyridin-2-yl) methyleneamino) phenoxy) phe-noxy)-N-((pyridin-2yl) methylene) benzenamine and 4-(4-(4-(Pyridin-2-yl)methylene amino) phenoxy)-N-((pyridin-2-yl)methylene) benzenamine. Their corrosion inhibitive efficiencies on MS have been tested in 1 M HCl medium through gravimetric and electrochemical measurements. Mirghasem Hosseini et al. [14] synthesized a pair of newly synthesized SB  $H_2A^4$ , N, N'-ortho-phenylene (salicylaldimine-2-hydroxy-1-naphthaldimine)] and [ $H_2A^3$ , N, N'-ortho-phenylene (salicylaldimine-acetylacetone imine). They were tested as inhibitors for MS corrosion in 0.5 M  $H_2SO_4$  solution. Results of weight loss, PDP and EIS measurements indicated excellent performance of these compounds as corrosion inhibitors. Using EIS, PDP, and linear polarization resistance tests, Hashim and co-authors [28] investigated a series of substituted benzylidene SBs for their inhibition efficiency on MS in 1 M HCl at 25 °C.

However, the imine group has poor hydrolytic stability at lower pH media[11]. The hydrolysis of SB corrosion inhibitors during corrosion testing in mineral acids has been studied in just few articles [11,15–17]. The hydrolysis of SB in aqueous solution has been documented in the literature for a wide range of pH values, and the fundamental properties of the hydrolysis

**Table 1** Physical properties of LPD compound.

Compound	Molecular Formula		Molecular weight				Color				Melting point (°C)				Yield	Rf
LPD	$C_{19}H_{20}N_2O_4$		340.38				Yellow				180 °C				90%	72%
	Solubility															
	Distilled water		Methanol		Ethanol		Chloroform		Dimethyl formamide		Dimethyl sulfoxide		Diethyl ether		Hexane	
	C	H	C	H	C	H	C	H	C	H	C	H	C	H	C	H
	IS	IS	IS	SS	IS	SS	S	S	S	S	S	S	IS	IS	IS	IS

C = Cool, H = hot, S = Soluble, SS = Slightly Soluble, IS = Insoluble.

mechanism are well recognized [11,18]. The imine group undergoes hydrolysis by regenerating an amine and an aldehyde which are the preceding compounds of SBs. So that using

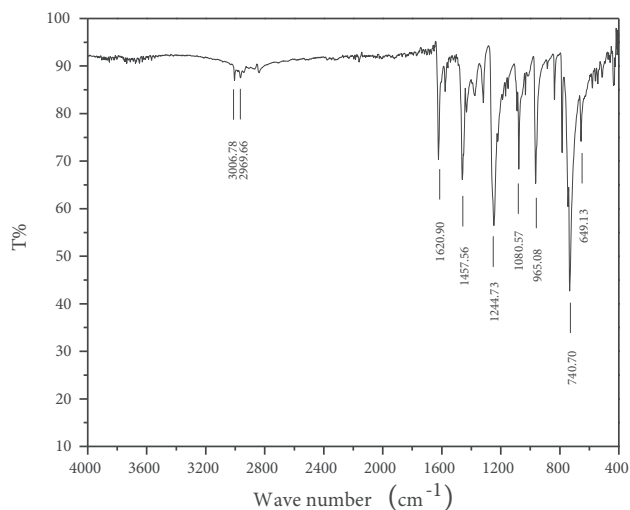


Fig. 1 FTIR Spectrum of LPD compound.

of SB as corrosion inhibitors in aqueous acid solutions is worthless unless their stability is confirmed in the tested corrosive media.

The objective of this study is to prepare a highly stable SB by condensation reaction between 1,3- propanediamine and o-Vanillin and testing its performance as corrosion inhibitor for MS in 1 M HCl acid. Spectroscopic techniques including UV, FTIR- and  $^1\text{H}$  &  $^{13}\text{C}$  NMR will be used to characterize the investigated SB compound. The stability of this compound will be confirmed firstly in the tested corrosive medium. Then the inhibition performance of LPD will be studied using gravimetric measurements and electrochemical techniques including PDP and EIS. The surface morphology and composition will be analyzed using FTIR, AFM, and SEM/EDS.

## 2. Experimental

The composition of MS as given by the supplier (Egyptian Iron and Steel Company) is 0.34% Mn, 0.004% Al, 0.09% Si, 0.013% S, 0.018% P, 0.08% C, and Fe has the remaining percentage. The used chemicals were of high grades. So that no further purification was required before using them.

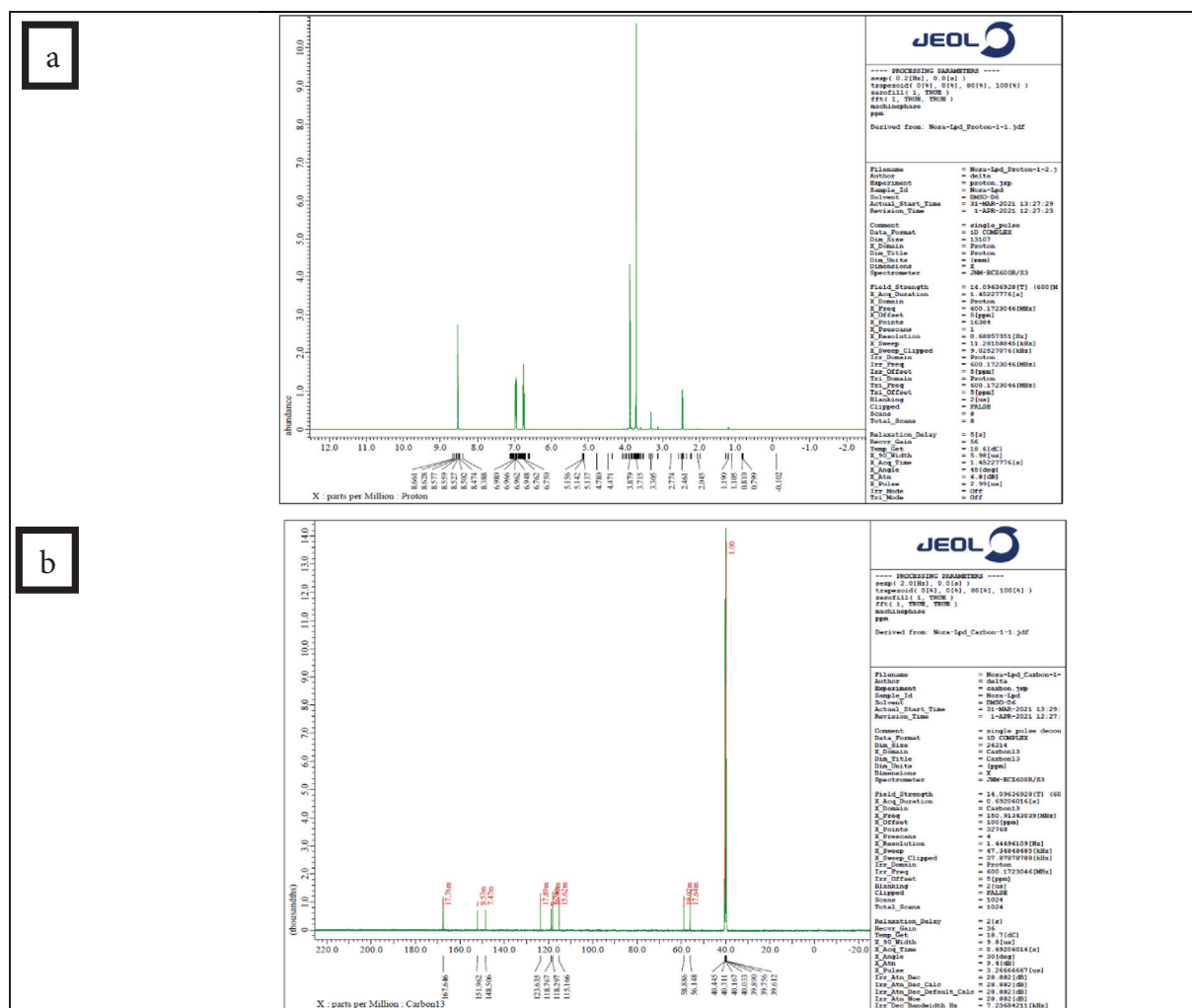
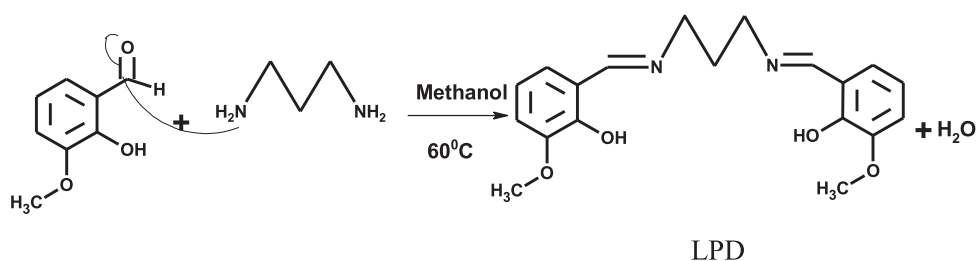


Fig. 2 [a] $^1\text{H}$  NMR and [b] $^{13}\text{C}$  NMR for LPD compound.

Synthesis of 2,2'-[propane-1,3-diylbis[azanylylidene (E) methanylylidene]]bis(6-methoxyphenol) (LPD) was carried out via the same method previously described [19], as depicted in equation (1). LPD compound was obtained by mixing 0.243 g (3.29 mmol) of 1,3-propanediamine dissolved in 10 ml of methanol and 2 g (0.486 m mol) of o-vanillin dissolved in 10 ml of methanol. This mixture was refluxed at 60 °C for two hours. A yellow precipitate was formed and collected by filtration. It was refined using cooled methanol and diethyl ether in repeated cleaning steps, then dried overnight..



Several techniques were used for characterization of LPD compound including Fourier transform infrared spectroscopy (FTIR) (8300 shimadzu spectrophotometer) that provided IR spectra in the wave number range (400–4000)  $\text{cm}^{-1}$  to verify the function groups present in the LPD compound and used also to detect LPD compound over MS surface after immersion in inhibited 1 M HCl solution. UV-Visible spectrophotometer (Agilent Technologies Cary 60 UV-Vis) was used to characterize LPD in solution and confirms its stability in 1 M HCl solution. Nuclear Magnetic Resonance Spectrometer 400 MHz (Avance Iii 400, Bruker, Germany) was used also to identify LPD structure.

The effectiveness of LPD as MS corrosion inhibitors in 1 M HCl solution has been examined. Two independent techniques were used to evaluate its inhibition efficiency. These include chemical methods such as gravimetric measurements and electrochemical methods such as potentiodynamic polarization (PDP) and electrochemical impedance spectroscopy (EIS).

The Mild Steel sheet was cut into 2 cm  $\times$  2 cm coupons. These coupons were polished by emery paper ranging in grade from 600 to 1000. These MS coupons were washed in ultrasonic water bath and then degreased in acetone. In the beginning, MS coupons were weighed by 4-digits analytical balance.

These coupons were then submerged thoroughly in a 100 ml beaker containing 1 M HCl solution without and with inhibitors at various time intervals and different temperatures. The coupons were removed and cleaned with water and acetone to eliminate any corrosion products. They were again dried and reweighed. Experiments were repeated to ensure the accuracy of the results, and the mean value of weight loss was indicated. The surface coverage ( $\theta$ ) and the inhibition efficiency (% I) were calculated by the following equations[20–21].

$$\theta = \frac{WL^* - WL}{WL^*} \quad (2)$$

$$\%I = \theta \times 100 \quad (3)$$

where  $WL^*$  and  $WL$  refers to the weight loss of MS specimen in uninhibited and inhibited 1 M HCl solution, respectively.

VersaSTAT 4 Potentiostat/Galvanostat with a built-in impedance analyzer was used for electrochemical studies. A 200 ml electrochemical cell had a three-electrode configuration, with MS sheets as the working electrode (3.14  $\text{cm}^2$ ), Saturated Calomel electrode as reference electrode, and graphite electrode as counter electrode. All electrochemical experiments were carried out at room temperature (25 °C).

Prior to electrochemical measurements, the working electrodes were allowed to stabilize in the test solution for 1 h. This period was enough to reach the stable potential known as equilibrium potential.

In potentiodynamic polarization experiments, the stabilized working electrode was polarized in both cathodic and anodic directions with a sweep rate of 0.17 mV/s. CView software version3.3b was used for data extraction concerning the polarization test. The values of corrosion current density ( $i_{\text{corr}}$ ),

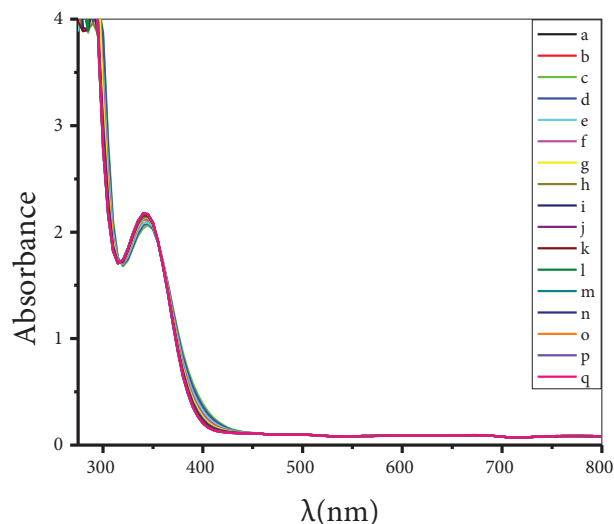


**Fig. 3** UV-Vis absorption spectra of LPD dissolved in DMF: H<sub>2</sub>O (4:1) solution (a) in 1 M HCl solution (b) in 1 M HCl solution every 5 min for 1 h (b–n) in 1 M HCl after 2 h (o) after 3 h (p) and after 24 h (q).

corrosion potential ( $E_{\text{corr}}$ ) and anodic and cathodic Tafel constants ( $\beta_a$  &  $\beta_c$ ) were calculated from the extrapolation of straight part of Tafel lines. The polarization resistance ( $R_p$ ), surface coverage ( $\theta$ ) and inhibition efficiency (%I) were calculated by the following equations[20–22].

$$R_p = \frac{\beta_a \beta_c}{2.303 i_{\text{corr}} (\beta_a + \beta_c)} \quad (4)$$

$$\theta = \frac{i_{\text{corr}}^* - i_{\text{corr}}}{i_{\text{corr}}^*} \quad (5)$$

$$\%I = \theta \times 100 \quad (6)$$

where  $i_{\text{corr}}^*$  and  $i_{\text{corr}}$  represents the corrosion current densities for uninhibited and inhibited 1 M HCl solution, respectively.

Electrochemical impedance spectroscopic measurements were established at OCP with a small alternating voltage perturbation (10 mV) that was applied on the cell over a frequency range of 10 KHz – 10 mHz. A proper equivalent circuit was employed to fit data obtained from the impedance spectra using ZView software version 3.2c.

The surface coverage ( $\theta$ ) and the inhibition efficiency (%I) were calculated in terms of charge transfer resistance ( $R_{\text{ct}}$ ) by the following equations[20].

$$\theta = \frac{R_{\text{ct}} - R_{\text{ct}}^*}{R_{\text{ct}}} \quad (7)$$

$$\%I = \theta \times 100 \quad (8)$$

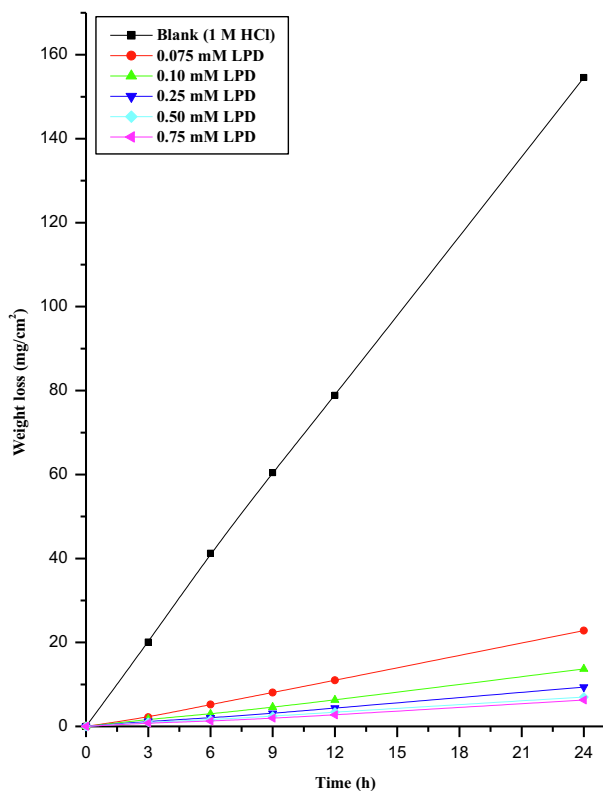


**Fig. 4** Variation of weight loss ( $\text{mg}/\text{cm}^2$ ) vs. time (h) for MS corrosion before and after addition of various LPD concentrations at 25 °C.

**Table 2** Values of surface coverage ( $\theta$ ) and inhibition efficiencies (%I) of LPD for corrosion of MS in 1 M HCl at 25 °C.

Immersion period (h)	LPD		
	Conc.	Surface coverage, $\theta$	Inhibition efficiency (%I)
3.00	0.075 mM	$0.891 \pm 0.01$	$89.06 \pm 1.38$
6.00		$0.873 \pm 0.03$	$87.31 \pm 2.56$
9.00		$0.867 \pm 0.01$	$86.66 \pm 1.17$
12.00		$0.860 \pm 0.02$	$86.05 \pm 1.77$
24.00	0.10 mM	$0.852 \pm 0.01$	$85.23 \pm 1.38$
3.00		$0.916 \pm 0.02$	$91.56 \pm 1.72$
6.00		$0.929 \pm 0.03$	$92.85 \pm 2.71$
9.00		$0.924 \pm 0.01$	$92.43 \pm 0.82$
12.00	0.25 mM	$0.920 \pm 0.01$	$92.04 \pm 1.44$
24.00		$0.911 \pm 0.01$	$91.15 \pm 1.26$
3.00		$0.939 \pm 0.05$	$93.89 \pm 5.40$
6.00		$0.951 \pm 0.02$	$95.05 \pm 2.08$
9.00	0.50 mM	$0.949 \pm 0.01$	$94.87 \pm 1.13$
12.00		$0.945 \pm 0.02$	$94.47 \pm 1.90$
24.00		$0.939 \pm 0.02$	$93.94 \pm 2.09$
3.00		$0.951 \pm 0.04$	$95.12 \pm 4.49$
6.00	0.75 mM	$0.962 \pm 0.03$	$96.18 \pm 2.72$
9.00		$0.959 \pm 0.01$	$95.95 \pm 1.11$
12.00		$0.957 \pm 0.02$	$95.70 \pm 2.16$
24.00		$0.955 \pm 0.01$	$95.48 \pm 1.15$
3.00	0.75 mM	$0.960 \pm 0.05$	$96.01 \pm 4.53$
6.00		$0.970 \pm 0.02$	$96.98 \pm 1.71$
9.00		$0.967 \pm 0.01$	$96.75 \pm 0.66$
12.00		$0.965 \pm 0.01$	$96.51 \pm 1.31$
24.00		$0.959 \pm 0.01$	$95.93 \pm 1.19$

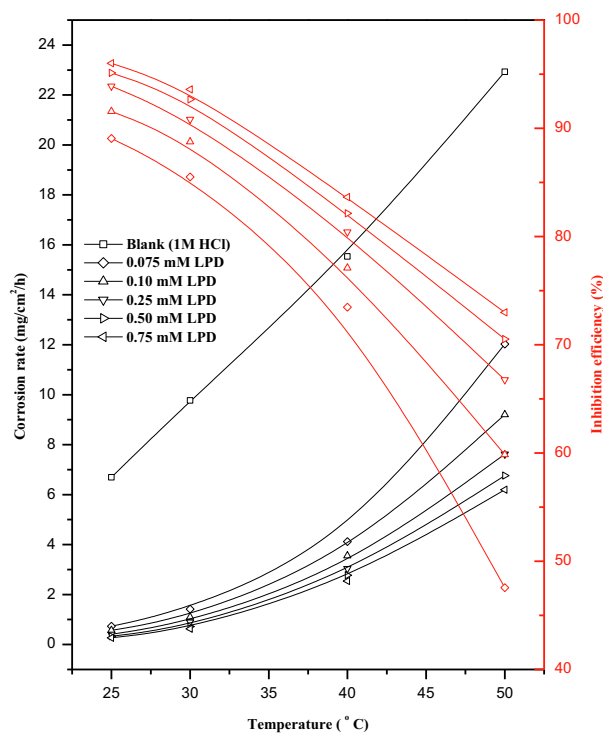


**Fig. 5** Change in corrosion rate ( $\text{mg}/\text{cm}^2/\text{h}$ ) and inhibition efficiency (%I) as a function of LPD concentration and temperature.



where  $R_{ct}^*$  and  $R_{ct}$  are the charge transfer resistances for uninhibited and inhibited 1 M HCl solution, respectively.

The influence of 1 M HCl solution without and with optimum concentration of LPD on both morphology and composition of MS surface were examined by using Scanning Electron Microscope/Energy Dispersive X-ray SEM/EDS (SEQuanta FEG 250 microscope provided with an EDX/ZAF quantifier) and Atomic Force Microscope AFM (Nano surface, model FlexAFM3) which is one of the most important instrumentation tools for surface topography characterization.

### 3. Results and discussions

#### 3.1. Characterization of LPD compound

The prepared LPD compound was characterized by its physical properties such as color, melting point, retention factor (Rf) and solubility. The physical properties of this compound were recorded in Table 1. These properties agree with that listed in literature [57–60]. This agreement confirms the identity of this compound. The purity was controlled by using TLC method and ( $\text{CH}_2\text{Cl}_2/\text{C}_2\text{H}_5\text{OH}$ ) as eluent. The calculated Rf value is equal to 72%.

FTIR spectra of LPD were used to characterize the existing functional groups as shown in Fig. 1. A strong band at about  $1280\text{ cm}^{-1}$  referred to C-O stretching frequency [23–25]. The weak broad band in the region  $2800\text{--}2700\text{ cm}^{-1}$ , which refers to the intramolecular hydrogen-bond O-H ... N = C [26–28]. A strong band at ( $1621\text{ cm}^{-1}$ ) confirms the presence of azomethine group ( $-\text{C} = \text{N} -$ ).

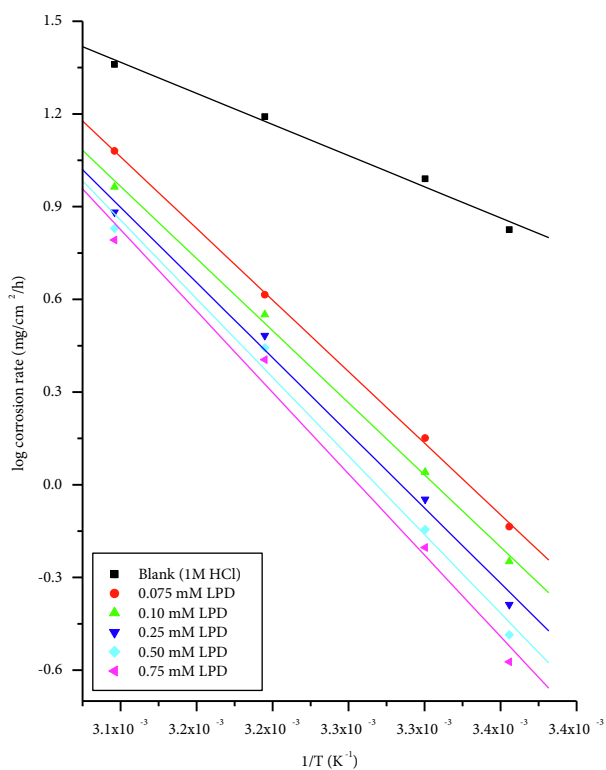


**Fig. 6** log corrosion rate vs.  $1/T$  for MS in 1 M HCl before and after addition of different LPD concentrations.

The peaks of the  $^1\text{H}$  NMR spectra of LPD are shown in Fig. 2-a. LPD exhibits a broad peak at 12–13 ppm due to the presence of phenolic protons. The integration is generally less than 2.0 due to the intramolecular hydrogen bond [23–25]. The signal of the azomethine ( $\text{HC} = \text{N}$ ) group is 8,54 ( $^1\text{H}$ ) ppm. The signals due to three aromatic protons (ArH) of vanillin have resonated as multiplets in the region 6.9–7.1 ppm, and signal at 3.3 ppm is due to three protons of methoxy group of *o*-vanillin [24–25]. The proton of  $=\text{N}-\text{CH}_2-\text{CH}_2-\text{N} =$  have resonated at 3.9 ppm as multiplet [24–25].

The  $^{13}\text{C}$  NMR results of LPD showed a sharp characteristic peak of azomethine carbon, that resonates at 166.68, 167.96 ppm and 164.45, respectively (Fig. 2-b). The signals observed at 115.97, 118.18, 123.87, 148.58, 152.66, 119.097, 119.84, 120.34, 120.34, 128.37 151.96, and 151, 96 ppm were

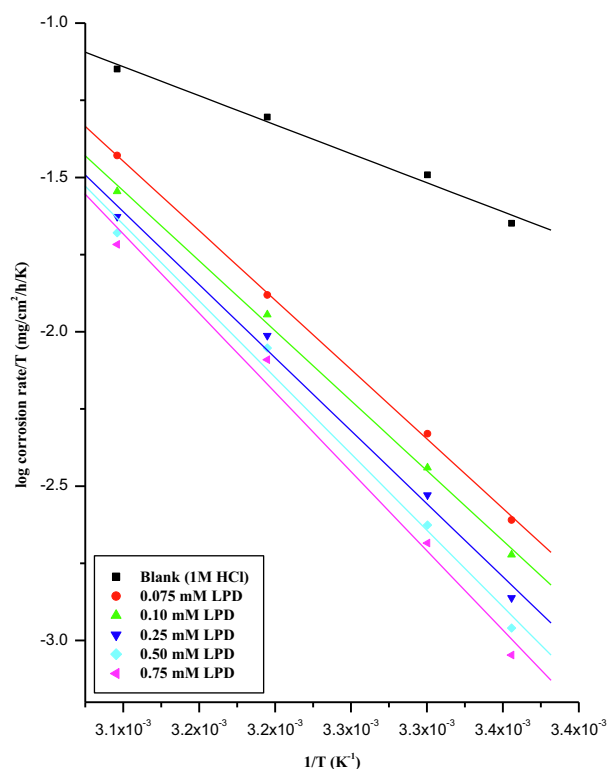


**Fig. 7** log corrosion rate/ $T$  ( $\text{mg}/\text{cm}^2/\text{h}/\text{K}$ ) vs.  $1/T$  for MS in 1 M HCl before and after addition of different LPD concentrations.

**Table 3** Activation parameters of MS dissolution in 1 M HCl without and with various concentrations of LPD compound.

Concentration	Activation parameters		
	$E_a^*$ , $\text{KJ mol}^{-1}$	$\Delta H^*$ , $\text{kJ mol}^{-1}$	$\Delta S^*$ , $\text{J mol}^{-1}\text{K}^{-1}$
1 M HCl	38.555	35.977	-107.80
0.075 mM	88.687	86.109	41.76
0.10 mM	89.346	86.768	41.96
0.25 mM	93.143	90.564	52.44
0.50 mM	97.386	94.808	64.80
0.75 mM	100.834	98.256	74.90

assigned for C = C(Ar) of ring of o-vanillin in LPD compound. The signals displayed at 56, 23, 55, 99, 58, 38, 56, 14, and 56.17 ppm was reasonably assigned to (CH<sub>3</sub>-O-), and the signals at 31,98 ppm belong to methyl carbon in LPD compound. The characteristic azomethine peak at 167.96 ppm [29].

In UV-Visible spectra of LPD, the bands observed in the range 305–445 nm and 220–260 nm are due to n – π\* transition of the imine group and π – π\* transition of the aromatic ring, respectively [30]. Typical absorption peaks of LPD were observed at 350 nm, whereas it is corresponding to n – π\* transition of C = N [31–32] as shown in Fig. 3.

### 3.2. Stability of LPD under experimental conditions

Many studies have reported that pH plays a key role in the hydrolytic stability of SB. However, significant hydrolysis may even take place at near-neutral pH conditions. The effect

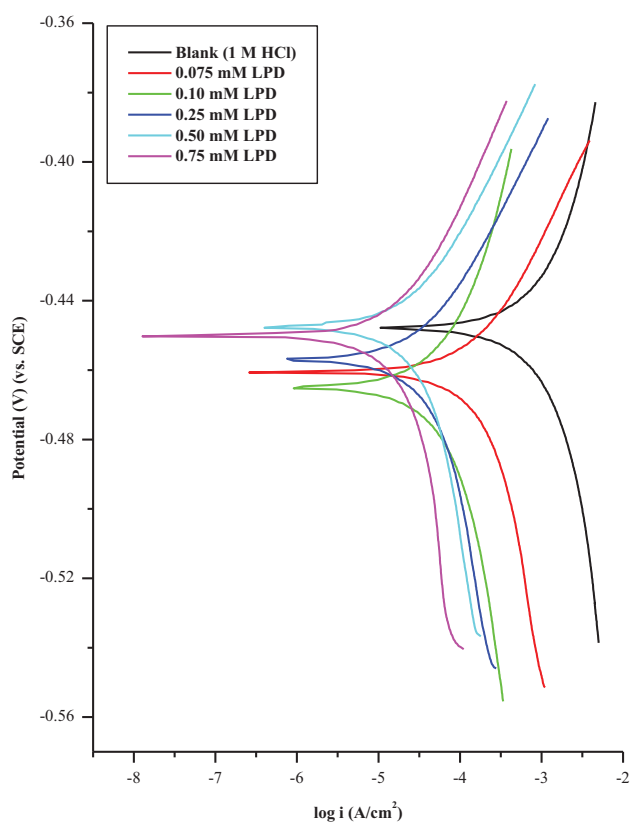


**Fig. 8** Tafel curves for MS corrosion in 1 M HCl before and after addition of various LPD concentrations at 25 °C.

of pH on the hydrolysis of LPD was determined by their UV–Vis absorption spectra. Because of the limited solubility of these ligands in water at 25 °C as shown in Table 1, their hydrolysis was studied in water–DMF mixture (20/80). In such mixture, LPD compound were sufficiently soluble. Fig. 3 illustrates the experimental UV–Vis. absorbance curves for stability test of LPD compound in 1 M HCl at 25 °C; no significant change occurs in 24 h. This indicates the stability of the imine function group of the ligand. This tetradentate SB ligands have two imine Bridges make them very stable. The proved stability of these ligands in 1 M HCl, increases their ability to be used as corrosion inhibitors.

### 3.3. Gravimetric measurements

The obtained weight loss-time curves for MS in 1 M HCl solution with and without different concentrations of LPD are shown in Fig. 4. The curves of LPD concentrations fall below that of the free acid. This suggests that the existence of these compounds slows the corrosion rate of MS in 1 M HCl solution, or these compounds function as corrosion inhibitors.

The concentration of LPD influences their inhibition ability. As a result, increasing the bulk concentration of these compounds, and therefore increasing the covered area of the metal surface, slows the corrosion of MS, as evidenced by the decrease in weight loss (mg/cm<sup>2</sup>).

The percentage inhibition of MS dissolution in 1 M HCl solution was determined after different time intervals for each tested LPD concentration. Table 2 shows the calculated values of surface coverage ( $\theta$ ) and percentage inhibition (%I) which demonstrated that when LPD concentration in the corrosive medium increases, its inhibitory effectiveness increases as well.

### 3.4. Effect of temperature

In the absence and presence of LPD compound, the rate of weight loss (mg/cm<sup>2</sup>/h) of MS in 1 M HCl solution was measured at different temperatures in the range (25–50 °C). Fig. 5 shows that as the temperature increases the corrosion rate in both blank and LPD additives solutions is shifted to higher value. However, in the presence of these LPD additives, the increase of corrosion rate occurs at slower rate than that in blank solution.

The increase of corrosion rate, as temperature increases, indicates that the inhibition efficiency of LPD compound decreases with rising temperature as shown also in Fig. 5. This means that the desorption of LPD is supported by rising temperature. This behavior proves that the inhibition of MS dissolution occurs by physical adsorption of LPD on the MS surface[33].

**Table 4** The effect of LPD concentrations on the electrochemical polarization parameters, surface coverage, and inhibition efficiency of MS corrosion in 1 M HCl solution at 25 °C.

Concn. (mM)	$E_{\text{corr.}}$ (mV)	$i_{\text{corr.}}$ ( $\mu\text{A}/\text{cm}^2$ )	$\beta_a$ (mV/dec)	$\beta_c$ (mV/dec)	$R_p$ ( $\pi \text{ cm}^2$ )	$\theta$	%I
0	$-441 \pm 3.05$	$1728.99 \pm 211.11$	$138.05 \pm 10.04$	$-203.68 \pm 13.34$	$20.66 \pm 1.48$	–	–
0.075	$-456 \pm 4.16$	$201.95 \pm 96.38$	$48.99 \pm 2.79$	$-99.25 \pm 9.75$	$70.53 \pm 3.80$	$0.90 \pm 0.03$	$90.42 \pm 3.35$
0.10	$-463 \pm 3.38$	$90.08 \pm 9.64$	$97.81 \pm 7.33$	$-124.56 \pm 9.69$	$264.10 \pm 14.80$	$0.96 \pm 0.05$	$95.51 \pm 5.47$
0.25	$-452 \pm 2.09$	$45.99 \pm 4.83$	$45.56 \pm 4.08$	$-110.41 \pm 7.86$	$304.50 \pm 16.25$	$0.98 \pm 0.06$	$97.63 \pm 6.21$
0.50	$-444 \pm 1.18$	$28.87 \pm 2.79$	$47.80 \pm 3.54$	$-106.25 \pm 5.42$	$495.79 \pm 18.00$	$0.98 \pm 0.04$	$98.30 \pm 3.84$
0.75	$-446 \pm 2.84$	$21.61 \pm 1.68$	$52.10 \pm 7.25$	$-78.89 \pm 3.64$	$630.42 \pm 19.25$	$0.99 \pm 0.05$	$99.07 \pm 5.33$

The activation energy ( $E_a^*$ ) required for MS dissolution reaction in inhibited and uninhibited 1 M HCl solution was determined using the following Arrhenius equation[20–21].

$$Rate = A e^{(-E_a^*/RT)}$$

Other thermodynamic parameters of activation such as entropy of activation ( $\Delta S^*$ ), and enthalpy of activation ( $\Delta H^*$ ) were determined using the following transition-state equation[20–21].

$$Rate = RT/N_{Ah} e^{(\Delta S^*/R)} e^{(\Delta H^*/RT)}$$

The frequency factor is A, the Avogadro's number is  $N_A$ , the Plank's constant is h, and the universal gas constant is R. The slopes of  $\log Rate$  vs.  $1/T$  and  $\log (Rate/T)$  vs.  $1/T$  are  $-E_a^*/2.303R$  and  $-\Delta H^*/2.303R$ , respectively. For the Arrhenius and transition state equations, the intercepts will be A and  $\log R/N_{Ah} + \Delta S^*/2.303R$ , respectively.

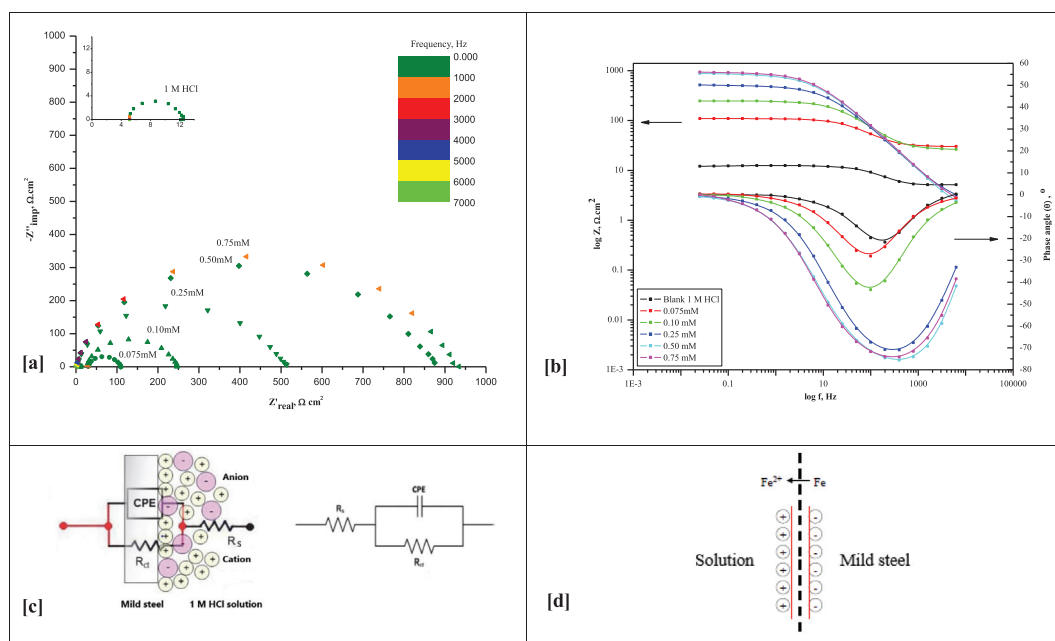


**Fig. 9** Nyquist (a) and Bode (b) plots of MS in 1 M HCl before and after addition of various LPD concentrations at 25 °C, the equivalent circuit (c) and schematic diagram of the mild steel-solution interface (d).

**Table 5** Physical processes of the equivalent circuit components.

Electrical circuit component	Physical process
Resistor $R_{ct}$	Charge-transfer or electron transfer resistance across the surface
Constant phase element, CPE	Electrical double layer capacitance
Resistor, $R_s$	Solution resistance (IR drop)

**Table 6** Impedance parameters for studied MS corrosion before and after addition of various LPD concentrations.

Concentration (ppm)	$R_s$ ( $\Omega \cdot \text{cm}^2$ )	$R_{ct}$ ( $\Omega \cdot \text{cm}^2$ )	$Y_0$ ( $\mu \Omega^{-1} \text{s}^n \cdot \text{cm}^{-2}$ )	n	$10^3 \chi^2$	$C_{dl}$ ( $\mu\text{F} \cdot \text{cm}^{-2}$ )	$\theta$	I%
1 M HCl	5.08 $\pm 0.25$	$7.26 \pm 0.47$	$367.31 \pm 17.19$	0.93 $\pm 0.01$	$6.45 \pm 0.27$	227.40 $\pm 17.07$	–	–
0.075 mM	9.48 $\pm 0.22$	$79.14 \pm 4.27$	$113.21 \pm 3.96$	0.85 $\pm 0.02$	$0.71 \pm 0.73$	$54.46 \pm 5.21$	0.91 $\pm 0.03$	90.82 $\pm 3.38$
0.10 mM	8.17 $\pm 0.32$	219.78 $\pm 22.74$	$70.81 \pm 3.88$	0.84 $\pm 0.01$	$0.92 \pm 0.22$	$33.39 \pm 2.46$	0.97 $\pm 0.03$	96.70 $\pm 2.56$
0.25 mM	2.23 $\pm 0.28$	491.86 $\pm 19.71$	$53.79 \pm 6.48$	0.86 $\pm 0.01$	$4.91 \pm 1.53$	$31.32 \pm 4.30$	0.99 $\pm 0.02$	$98.52 \pm 1.8$
0.50 mM	1.35 $\pm 0.13$	827.83 $\pm 37.56$	$48.34 \pm 7.83$	0.87 $\pm 0.01$	13.15 $\pm 3.13$	$31.32 \pm 5.03$	0.99 $\pm 0.03$	$99.12 \pm 2.7$
0.75 mM	1.73 $\pm 0.73$	889.43 $\pm 56.16$	$48.12 \pm 2.88$	0.87 $\pm 0.02$	$6.87 \pm 0.31$	$30.82 \pm 2.96$	0.99 $\pm 0.02$	99.18 $\pm 2.34$



**Table 7** The applied isotherm models[83,84].

Isotherm model	Linear form equation	Figure axis
Langmiur	$\frac{C}{\theta} = \frac{1}{K_{ads}} + C$	$\frac{C}{\theta}$ vs. C
Freundlich	$\log \theta = n \log C + \log K_{ads}$	$\log \theta$ vs. $\log C$
Temkin	$\theta = \left(\frac{2.303}{a}\right)(\log K_{ads} + \log C)$	$\theta$ vs. $\log C$
Flory-Huggins	$\log \frac{\theta}{C} = x \log(1 - \theta) + \log(xK_{ads})$	$\log \left(\frac{\theta}{C}\right)$ vs. $\log(1 - \theta)$
Frumkin	$\ln \left[\frac{\theta}{(1-\theta)C}\right] = \ln K + 2\alpha\theta$	$\ln \left[\frac{\theta}{(1-\theta)C}\right]$ vs. $\theta$
El-Awady	$\log \frac{\theta}{1-\theta} = y \log C + \log K$	$\log \left(\frac{\theta}{1-\theta}\right)$ vs. $\log C$

Plots of  $\log$  rate vs.  $1/T$  and  $\log$  (rate/ $T$ ) vs.  $1/T$  data are shown in Figs. 6 and 7. Table 3 shows the computed values of  $E_a^*$ ,  $\Delta S^*$ , and  $\Delta H^*$ .

The nearly same values of  $E_a^*$  indicate that the action of inhibitors follow a comparable mechanism, and the order of efficiency is linked to several factors such as steric effects, concentration, and characteristics of metal surfaces that are further related to preexponential factor (A).

The activation energy calculated for blank solution is 38.6  $\text{KJ mol}^{-1}$ , which is on the same order of magnitude as that

recorded by K.R. Ansari and M.A. Quraishi., 24.5  $\text{KJ mol}^{-1}$ , for MS corrosion in 1 M HCl solution [34] and 32.91  $\text{KJ mol}^{-1}$  in 20%  $\text{H}_2\text{SO}_4$  [35] and by P.M. Dasami et al., 37.33  $\text{KJ mol}^{-1}$  for the corrosion of MS in 1 M  $\text{H}_2\text{SO}_4$  solution[36].

The activation energy ( $\Delta E^*$ ) in the presence of LPD is greater than that in their absence. This refers to the retardation of corrosion rate in the presence of LPD compound.

Also, the entropy of activation ( $\Delta S^*$ ) in the presence of LPD is greater than that in their absence, and has negative values. This indicates that as it moves from reactants to activated complex, the degree of disordering decrease[33].

The LPD concentration has a direct relationship with  $\Delta S^*$ . This phenomenon was previously discussed for solutions without inhibitors as the transient state of the rate-determining step is more orderly than the initial state resulting in a negative value for  $\Delta S^*$ . An increase in  $\Delta S^*$  values is observed in the presence of inhibitor as the system moves from a less ordered to a more random structure[33].

### 3.5. Potentiodynamic polarization technique

The effect of the concentration of LPD on the current-potential relations of MS in 1 M HCl solution at 25 °C is illustrated in Fig. 8. Table 4 shows the relationship between the concentrations of LPD compound and the numerical values

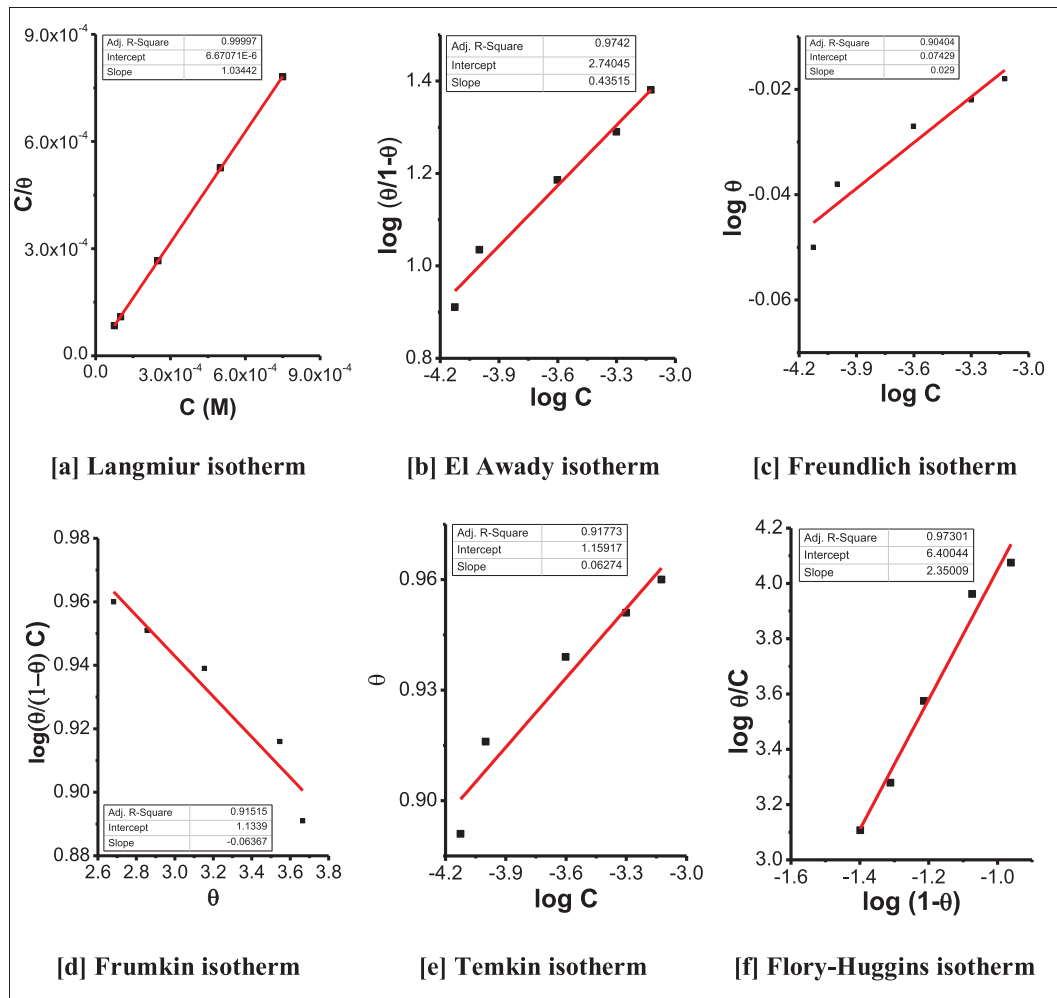


**Fig. 10** Isotherms for the adsorption of LPD compound on the MS surface in 1 M HCl using data from gravimetric method at 25 °C.

of corrosion current density ( $i_{\text{corr}}$ ), corrosion potential ( $E_{\text{corr}}$ ), surface coverage ( $\theta$ ), protection efficiency (%I) and Tafel slopes ( $\beta_a$  &  $\beta_c$ ). The results show that, the addition of LPD compound induced an increase in both cathodic and anodic overvoltage which depends upon concentration.

The difference between  $E_{\text{corr}}$  values that determined in absence and presence of LPD compound is less than 85 mV. As a result, these compounds function as a mixed-type inhibitor by slowing the cathodic process (hydrogen evolution) and anodic process (metal dissolution)[37–38].

The slopes of the anodic ( $\beta_a$ ) and cathodic ( $\beta_c$ ) Tafel lines are nearly constant and unaffected by LPD concentration. This indicates that LPD molecules have no impact on the mechanism of MS dissolution[21]. The  $i_{\text{corr}}$  values calculated from both the cathodic and anodic curves decreased. This demonstrates the adsorbing of LPD molecules on the MS surface, generating a protective layer against acid attack. The values of inhibition percentage (%I) that obtained from gravimetric and polarization measurements are obviously in a good agreement.

### 3.6. Electrochemical impedance spectroscopy

Fig. 9 show the impedance spectra for MS corrosion in 1 M HCl solution with and without LPD compound. In Nyquist

plot, as the concentration of LPD increases, the semicircle diameter becomes longer. The deviation from ideal semicircle is due to the corrosion induced roughness and inhomogeneity of the MS electrode surface. It is obvious that the profile of the impedance complex plane does not change with changing LPD concentration. These results display that adsorption of LPD in the double layer has no effect on the mechanism of the corrosion of the MS in 1 M HCl solution[20].

The corrosion process comprises several simultaneous physical processes and so, the equivalent circuit is composed of numerous circuit elements as depicted in Fig. 9c. Table 5 shows the relationship between these physical processes and EIS electrical circuit components.  $R_s$  represents the solution's pure ohmic resistance.  $R_{ct}$  stands for charge-transfer resistance, which is inversely related to corrosion rate and is a measure of electron transfer across the surface.

Positively charged ions are dissolved in solution throughout the corrosion process, whereas excess electrons are stored in the steel-lattice. As demonstrated in Fig. 9d, negative charge accumulates on the mild steel surface, attracting positively charged ions from solution. As a result, an electronegative front is formed on the mild steel surface, that opposed by an electropositive front in the solution. As a result of this charge arrangement, the interface works as a capacitor, and the capacitance associated with this interface is known as the dou-

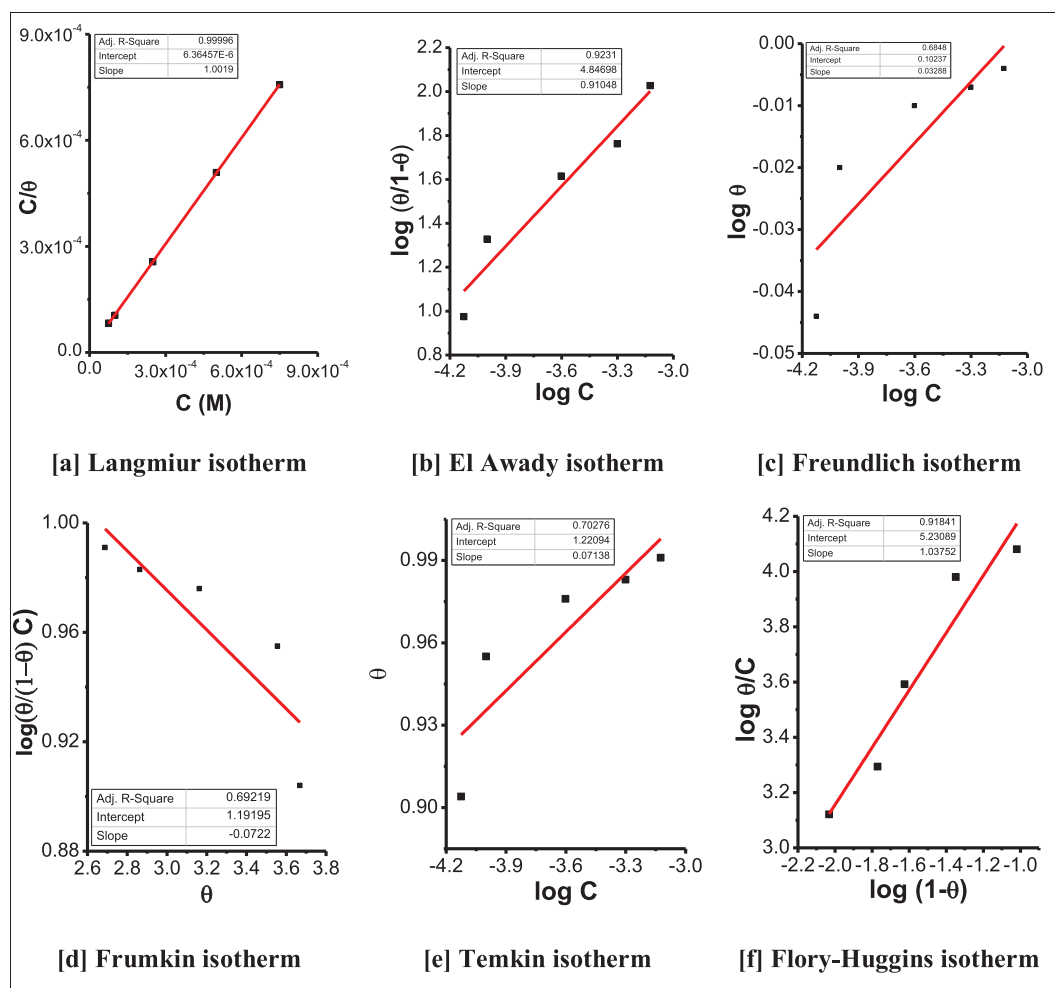


Fig. 11 Isotherms for the adsorption of LPD compound on the MS surface in 1 M HCl using data from PDP method at 25 °C.

ble layer capacitance,  $C_{dl}$  [39]. The constant phase element, CPE, is introduced in the circuit instead of a pure double layer capacitor to give a more accurate fit. CPE is used to recompense the effects of inhomogeneity and roughness of the MS surface. The equivalent impedance for CPE is calculated by Eq. (11)[20].

$$Z_{CPE} = Y_0^{-1}(j\omega)^{-n}$$

The CPE constant is  $Y_0$ , and the CPE exponent is  $n$ , which corresponds to the phase shift. The value of  $n$  is laying between 0 and 1. It indicates the degree to which the system deviates from the ideal case.

Table 6 lists the computed values of the impedance parameters of Nyquist plots at different concentrations of LPD compound. After adding LPD compound to the acidic solution, the surface heterogeneity decreases owing to the inhibitor adsorption on the MS surface, resulting in a slightly rise in the  $n$  value. The calculated fit goodness ( $\chi^2$ ) values for LPD are ranged from 0.0007 to 0.0131, respectively. This confirms that the equivalent circuit elements match the experimental data well.

The values of ( $R_{ct}$ ) clearly increased as the concentration of LPD increased, demonstrating MS corrosion inhibition in 1 M HCl solution. The inhibition percentage estimated using EIS is

comparable to that calculated using PDP and gravimetric measurements.

Eq. (12) is used to calculate the double layer capacitance ( $C_{dl}$ )[20].

$$Cdl = \frac{(Y_0 R_{ct})^{1/n}}{R_{ct}} \quad (12)$$

As LPD concentration increases,  $C_{dl}$  values fall. Helmholtz model of electrical double layer gives a correlation between  $C_{dl}$  to the electrode surface area ( $S$ ), the electrical double layer thickness ( $\delta$ ), the medium dielectric constant ( $\epsilon_0$ ) and the permittivity of vacuum ( $\epsilon$ ) as illustrated in Eq. (13)[20].

$$Cdl = \frac{\epsilon_0 \epsilon}{\delta} S \quad (13)$$

The development of an adsorbed layer of LPD at the electrode surface results in a drop in the  $C_{dl}$  value due to an increase in  $\delta$  or a decrease in  $\epsilon_0$ .

The interfacial impedance seemed to rise on the Bode plot when the concentration of LPD was raised. The phase angle ( $\theta$ ) plot revealed a single peak, indicating a single time constant for the interfacial corrosion process[40]. The greater the negative phase angle ( $\theta$ ), the higher the interfacial capacitance due to adsorption of LPD molecules to the electrode surface[41].

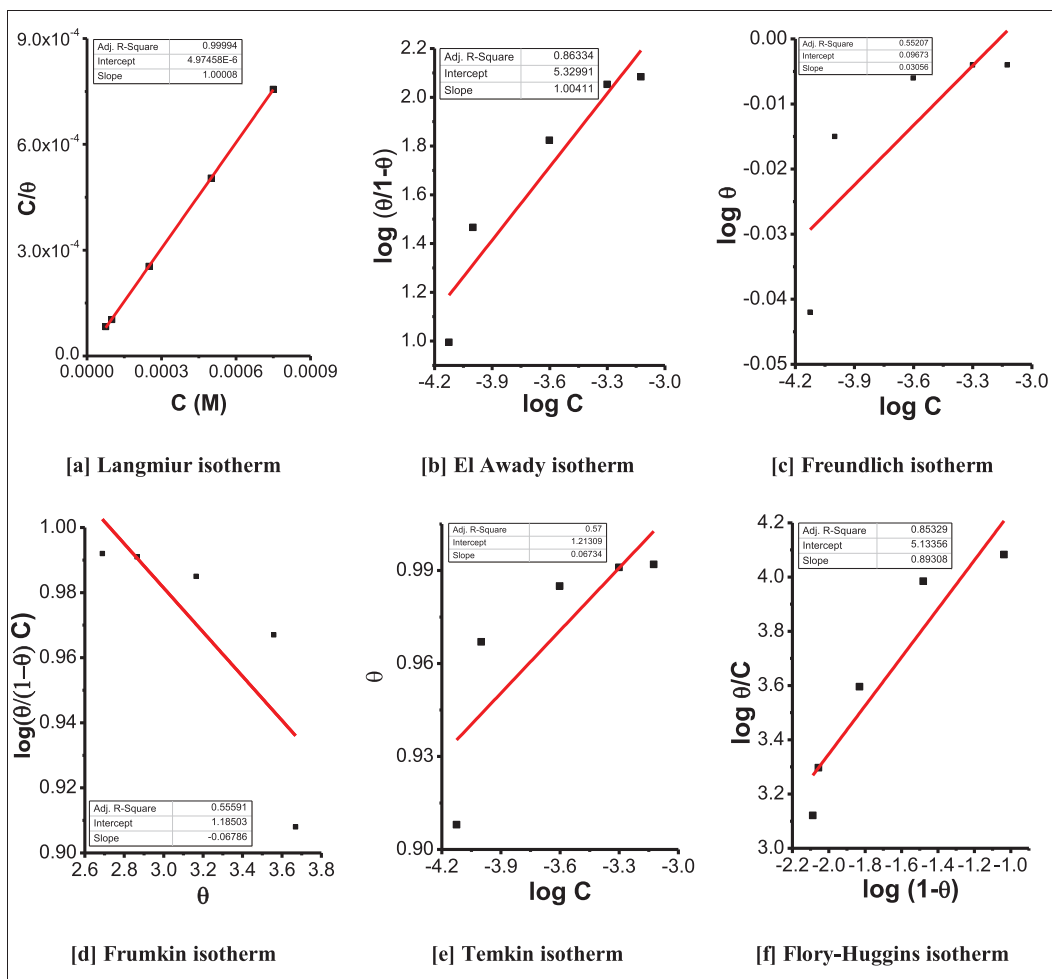
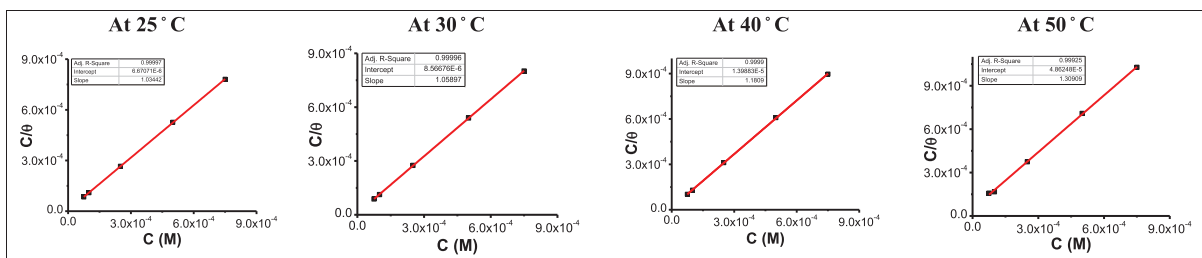


Fig. 12 Isotherms for the adsorption of LPD compound on the MS surface in 1 M HCl using data from EIS method at 25 °C.



**Fig. 13** Langmuir isotherm for the adsorption of the investigated SBs on the MS surface in 1 M HCl at different temperatures.

### 3.7. Adsorption isotherm

The adsorption of inhibitor molecules on the metal surface can be proceed through physical or chemical adsorption mechanisms. The border line between the two mechanisms of adsorption is often indistinct. But some experimental results make this possible. Physical adsorption of LPD molecules on MS surfaces is suggested by a reduction in inhibitory action with increasing temperature, as demonstrated in Fig. 5, while the reverse behaviour suggests the chemical adsorption.

The most appropriate adsorption isotherm can describe the interaction between the inhibitor molecules and the metal surface through prediction of the mode of adsorption if it is physical or chemical.

A general mathematical adsorption isotherm expression is given by the form[42]:

$$f(\theta, x) \exp(-a, \theta) = KC$$

where, K is the equilibrium constant of the adsorption process,  $f(\theta, x)$  is a factor related to configuration that substantially depends on the proposed physical model and assumptions supporting the isotherm derivation, and  $a$  is a molecular interaction parameter that depends on the degree of molecular interactions and surface non-uniformity of the adsorbed layer[42].

A number of adsorption isotherms such as Langmuir, Temkin, Freundlich, Flory-Huggins, Frumkin, and kinetic-thermodynamic (El-Awady) model have been proposed to suit the experimental data of the current work obtained by all measurements. The choice of the most appropriate model depends on the correlation coefficient value of the fitted line after graphical representation of the linear form equations that are listed in Table 7 as shown in Figs. 10-12.

Among the isotherms considered above, the most adequate one for the obtained experimental data was Langmuir model where correlation coefficient value was equal to  $\approx 1.0$  for all results obtained by chemical and electrochemical methods.

According to Langmuir model, the inhibitor concentration ( $C_{inh}$ ) is directly related to  $\theta$  parameter[20].

$$C/\theta = 1/K_{ads} + C_{inh}$$

where  $K_{ads}$  is the equilibrium constant of adsorption.

Plots of  $C_{inh}/\theta$  against  $C_{inh}$  for adsorption of LPD molecules on MS surface at 25°, 30°, 40°, and 50 °C are shown in Fig. 13. The data gave straight lines confirming that Langmuir's isotherm is valid to describe the adsorption behavior of LPD on MS surface. For the ideal scenario of chemical and physical modes of adsorption on a flat surface without any interaction between the molecules that have been adsorbed, Langmuir's isotherm is used.

The standard adsorption free energy ( $\Delta G_{ads}^\circ$ ) is related to  $K_{ads}$  by Eq. (16)[20].

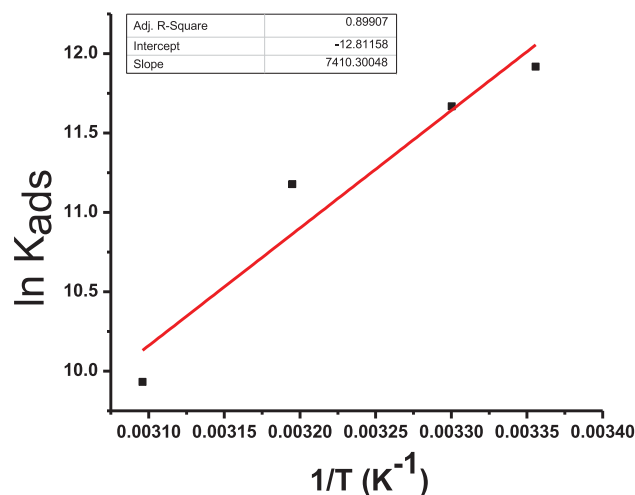


**Fig. 14**  $\ln K_{ads}$  vs.  $1/T$  for adsorption of LPD on the MS surface in 1 M HCl.

**Table 8** Adsorption thermodynamic parameters for LPD on MS surface.

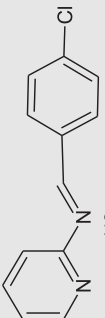
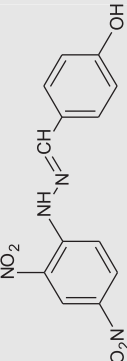
Thermodynamic parameters					
Method	Temperature, °C	$K_{ads}$	$\Delta G_{ads}^\circ$ , KJ mol <sup>-1</sup>	$\Delta H_{ads}^\circ$ , KJ mol <sup>-1</sup>	$\Delta S_{ads}^\circ$ , J mol <sup>-1</sup>
Gravimetric	25	149909.08	-39.48	-61.61	-73.13
PDP	25	157119.81	-39.60		
EIS	25	201022.00	-40.21		
Gravimetric	30	116730.25	-39.51		
Gravimetric	40	71488.32	-39.54		
Gravimetric	50	20565.64	-37.46		

**Table 9** Comparison between the results of LPD compound and other organic inhibitors for corrosion of MS in acidic media.

Inhibitor	Structure	Corrosive medium	Methods	Characteristics of inhibitor				
				Inhibition %	Adsorption model	Adsorption type	Inhibitor type	Reference
2,2'-{propane-1,3-diylbis[azanylylidene(E) methanylylidene]}bis(6-methoxyphenol)		1 M HCL	Weight loss, OCP, PDP, and EIS	95.93% at 25 °C	Langmuir	physisorption and chemisorption	Mixed type	Present study
4,4'-bis(2,4-dihydroxybenzaldehyde) diphenylethanediiimine		1 M HCL	Weight loss, OCP, PDP, and EIS	95.58% at 30 °C	Langmuir	Physisorption	Mixed type	[40]
1-phenethyl-3-(3-phenoxypropyl)-1H-imidazol-3-ium bromide ([Imid-3PE] Br)		1 M HCL	OCP, PDP, and EIS	96.8% at 25 °C	Langmuir	Physisorption	Mixed type	[41]
Isophthalohydrazideisophthalo-hydrazide		1 M HCL	Weight loss	96.4 % at 30 °C	Langmuir	Chemisorption	Mixed type	[42]
1-Hexyl-3- methylimidazolium iodide		1 M HCL	OCP, PDP and EIS	93.6% at 25 °C	Langmuir	Physisorption	Mixed type	[43]
4-((2,3-dichlorobenzylidene)amino)-3-methyl-1H-1,2,4-triazole-5(4H)-thione		1 M HCL	Weight loss PDP EIS	97.3% at 30 °C	Langmuir	physisorption and chemisorption	Mixed type	[44]

(continued on next page)

**Table 9** (continued)

Inhibitor	Structure	Corrosive medium	Methods	Characteristics of inhibitor			Reference
				Inhibition %	Adsorption model	Adsorption type	
(4-Chloro-benzylidene)-pyridine-2-yl)-amine		1 M HCl	Weight loss PDP EIS	99.5% at 25 °C	Langmuir	physisorption	Mixed type [45]
(E)-4-(2-(2,4-dinitrophenyl)hydrazono)methyl phenol		1 M HCl	Weight loss PDP EIS	89% at 27 °C	Langmuir	physisorption and chemisorption	Mixed type [46]

$$K_{ads} = 1/55.5 e^{-\Delta G_{ads}^{\circ}/RT}$$

where T is the absolute temperature, R is the universal gas constant and 55.5 is the water molar concentration in solution.

The values of the thermodynamic parameters  $K_{ads}$  and  $\Delta G_{ads}^{\circ}$  are listed in Table 8. The negative sign of  $\Delta G_{ads}^{\circ}$  value refers to the spontaneity of the adsorption of LPD molecules on MS surface.

Generally, if  $\Delta G_{ads}^{\circ}$  value is  $-20$  kJ/mol or less negative, adsorption will be associated with physisorption, and it involves electrostatic interactions between charged metal surface and charged molecules of inhibitor. On the other hand, the adsorption process is referred as chemisorption, when  $\Delta G_{ads}^{\circ}$  values are  $-40$  kJ/mol or more negative and the inhibitor molecule and metal surface share charge to create a chemical bond[43].

The obtained  $\Delta G_{ads}^{\circ}$  values for LPD compound had  $\Delta G_{ads}^{\circ}$  values ranged between  $-20$  and  $-40$  kJ/mol. So that both physisorption and chemisorption were incorporated in the adsorption process of LPD on MS surface.

Fig. 14 gives a plot of  $\ln K_{ads}$  vs. reciprocal of absolute temperature for the adsorption of LPD on MS surface. The slope and intercept of the obtained straight lines can be used in calculation of the standard enthalpy change of adsorption ( $\Delta H_{ads}^{\circ}$ ) and standard entropy change of adsorption ( $\Delta S_{ads}^{\circ}$ ) using the following equation[44–45]:

$$\ln K_{ads} = \frac{-\Delta H_{ads}^{\circ}}{RT} + \frac{\Delta S_{ads}^{\circ}}{R} - \ln 55.5 \quad (17)$$

This equation is derived from Eq. (15), and the basic thermodynamic equation given below[44–46].

$$\Delta G_{ads}^{\circ} = \Delta H_{ads}^{\circ} - T\Delta S_{ads}^{\circ} \quad (18)$$

The obtained values of  $\Delta H_{ads}^{\circ}$  and  $\Delta S_{ads}^{\circ}$  are listed in Table 8. The negative value of  $\Delta H_{ads}^{\circ}$  indicates the exothermic nature of the adsorption process, confirming desorption of some inhibitor molecules with increasing temperature, which leads to decrease in  $K_{ads}$  values. Generally, in an adsorption process, endothermic nature specifies chemisorption, but exothermic nature indicates either physisorption or chemisorption. On the other hand, the values of  $\Delta S_{ads}^{\circ}$  are negative due to the decrease in the entropy owing to the arrangement of LPD molecules on MS surface rather than their free motion in the solution[46].

### 3.8. Comparative study

In comparison to the published data that is illustrated in Table 9, the examined LPD compound may be deemed as a powerful corrosion inhibitor for MS in acidic environment based on its protection efficiency with a maximum value of 95.93 percent after 24 h immersion. The current study's findings are consistent with those reported in the previous studies. That used different types of SB ligands or even other categories of organic compounds as corrosion inhibitors. The findings showed that Langmuir model is specified as a common adsorption model, as well as categorization as a mixed-type inhibitor.

### 3.9. Surface morphology and composition

#### 3.9.1. AFM examination

The atomic force microscope is an extremely effective tool for analyzing microstructure. Surface roughness was quantified on



area scales of  $10\ \mu\text{m} \times 10\ \mu\text{m}$ . Fig. 15 shows two and three-dimensional AFM images of polished MS surface, immersed MS surface in 1.0 M HCl and in HCl solution containing optimum concentrations of LPD. The average roughness ( $S_a$ ) of MS polished sample is 71 nm which increased after immersion in 1.0 M HCl to be 156 nm. As a result of acid assault on the MS surface and formation of cracks and cavities distributed on it. The surface of MS suffers far less damage when LPD is present, the value of  $S_a$  is about 128 nm.

### 3.9.2. SEM/EDX examination

Table 10 depicts the morphology of MS surface before and after immersion in solutions with or without the investigated inhibitor. The SEM photo of the abraded metal surface shows only polishing scratches and no flaws are visible but after immersion for 24 h in blank solution, SEM images reveal a rust layer with cavities and cracks that covering the whole metal surface. A smooth surface appeared when the optimum concentration of LPD was added to the acidic solution. This implied the formation of a protective film on the MS surface and reduction of the corrosion rate.

The EDX spectra of MS surfaces are also shown in Table 10. It gives the composition in percentage of elements as Mn, C, Cl, Fe, O, and N. The presence of chlorine and oxygen could be associated with the formation of compounds such as  $\text{FeCl}_2$ ,  $\text{Fe}_2\text{O}_3$ ,  $\text{Fe}_3\text{O}_4$  as corrosion products[47]. The addition of LPD lowered the concentration of Cl at MS surface from 12.84 percent in the blank solution to 6.77 percent. The oxygen to iron ratio was similarly reduced once LPD were added. This supports the inhibitory characteristics of these compounds against corrosion of MS in 1 M HCl.

### 3.9.3. FTIR spectra

The functional groups included in the chemical structure of LPD were verified using FTIR spectra to have a better understanding of how this compound interact with MS surface. The FTIR spectra illustrated in Fig. 16 showed a significant wide band at  $3600\ \text{cm}^{-1}$  indicating the existence of water molecules[48]. At  $2926\ \text{cm}^{-1}$  and  $2855\ \text{cm}^{-1}$ , the C–H asymmetric and symmetric stretching vibrations were appeared. The existence of an azomethine group ( $\text{C} = \text{N}$ ) is attributed to the band ( $1616\text{--}1625\ \text{cm}^{-1}$ ), which validates the adsorption of LPD on MS surface. The appearance of a new absorption band at  $552\ \text{cm}^{-1}$  was attributed to N–Fe and O–Fe, as well as a shift of the absorption band for the  $\text{N} = \text{C}$  band up to  $1550\text{--}1600\ \text{cm}^{-1}$  compared to LPD itself, confirmed the adsorption of LPD molecules on the MS surface and creation of a complex with Fe atoms on MS surface[49].

### 3.10. Corrosion inhibition mechanism

Explanation of the inhibition process necessitates thorough understanding of the protective organic inhibitor's interaction with the metal surface. The MS surface is positively charged in hydrochloric acid [50]. LPD molecules exist in hydrochloric acid solution as neutral molecules or as positively charged ions. The probability of complex formation between LPD and the metal ions resulting from MS dissolution in 1 M HCl solution was examined. The UV-Vis spectra of the tested acidic solution containing LPD before and after MS coupons immersion were measured and illustrated in Fig. 17. There is no shift in the absorption bands before and after the immersion of these MS coupons in the tested

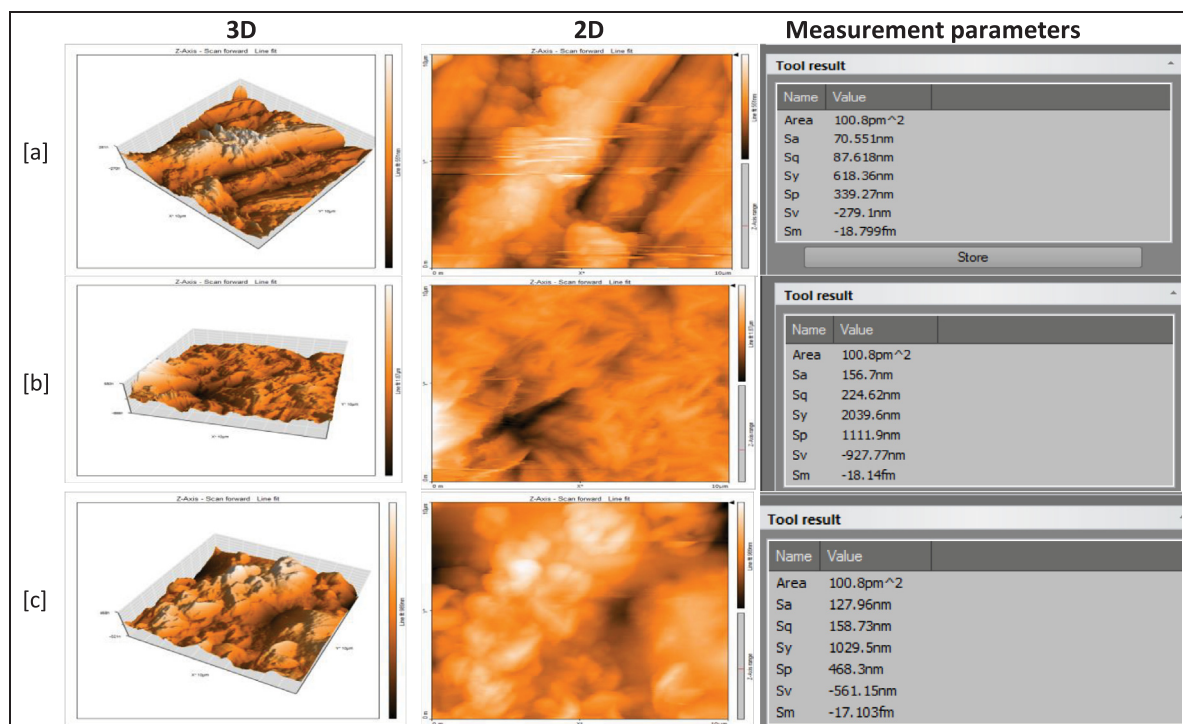
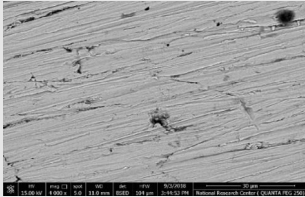
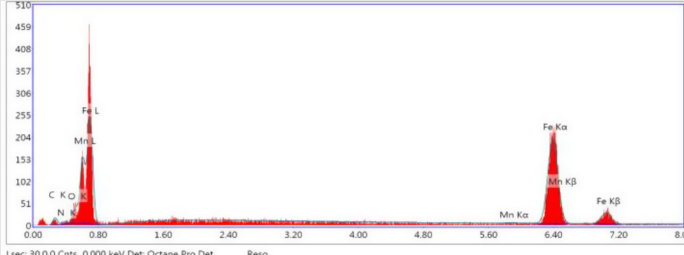
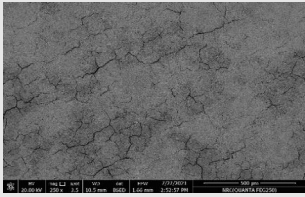
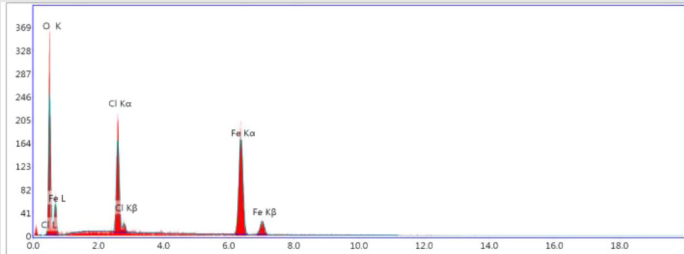
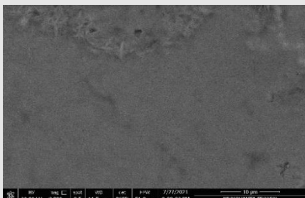
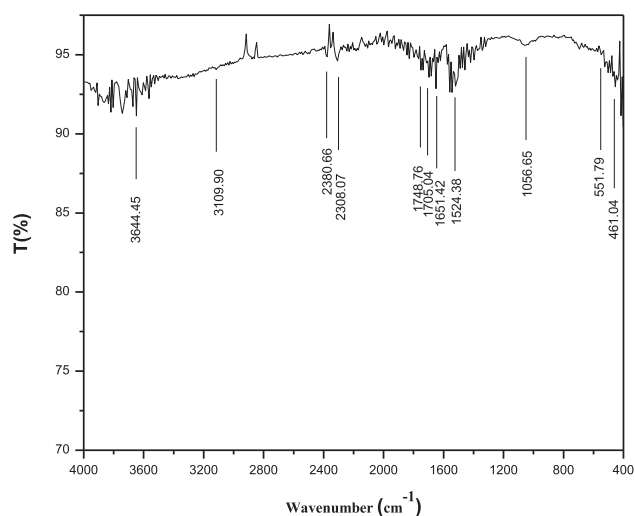
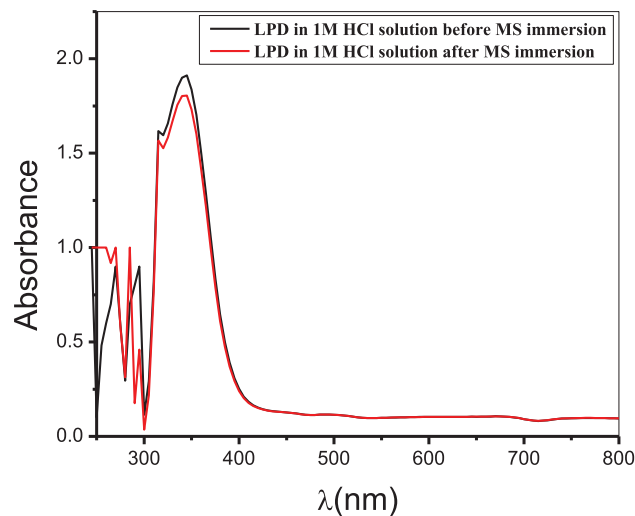


Fig. 15 Two- and Three-dimensional images of (a) polished MS surface and MS surfaces after 24 h immersion (b) in 1 M HCl (c) in 0.75 mM LPD.

**Table 10** SEM images of MS surface and associated EDX spectra.

Sample	SEM	EDX	Element	Weight %
Polished Coupon			C	10.62
			N	4.86
			O	8.41
			Mn	0.09
Blank			O	35.71
			Cl	12.84
			Fe	51.45
			LPD compound	
N	0.98			
O	37.43			
Cl	6.77			
Fe	54.77			

**Fig. 16** MS surface layer's FTIR spectrum after 24 h immersion in 1 M HCl and in 1 M HCl + 0.75 mM LPD.**Fig. 17** UV-Vis absorption spectra of LPD in 1 M HCl solution before and after MS coupons immersion for 24 h.

solutions. This confirms that there is no complex formation and LPD present free in solution. As shown in Fig. 18, one or more of the following mechanisms can be used to describe the adsorption of LPD molecules on the interface of MS/acid solution: (i) Electrostatic attraction between pro-

tonated LPD molecules with the adsorbed  $\text{Cl}^-$  ions, (ii) interactions between the aromatic rings ( $\pi$ -electrons) and empty d-orbitals of Fe atoms, and (iii) interaction between lone pairs of electrons (non-bonding) of heteroatoms and empty d-orbitals of Fe atoms.

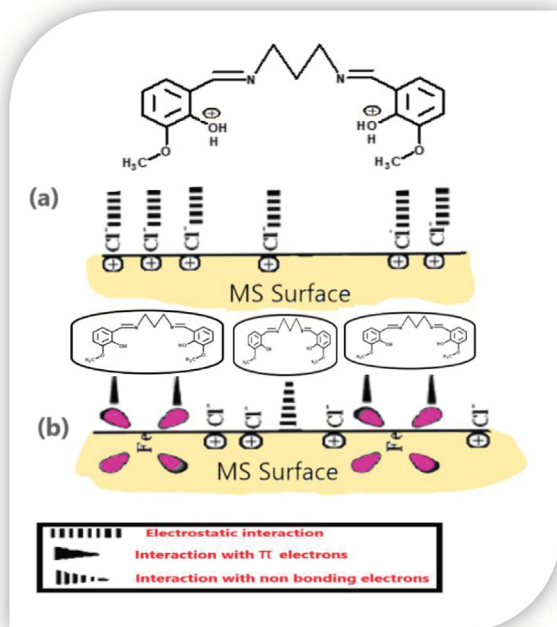


**Fig. 18** Schematic representation of adsorption types (a) physical and (b) chemical of LPD on MS surface.

#### 4. Conclusion

The present work represents a study on using LPD as inhibitor for MS corrosion in 1 M HCl. Its inhibition ability was tested using gravimetric, PDP, and EIS measurements after examination of their stability in the acidic corrosive medium using UV-visible spectroscopy. The calculated inhibition efficiency was 95.93 % for 0.75 mM LPD after 24 h of immersion at 25 °C. The adsorption process of LPD on MS surface was discussed and its related thermodynamic parameters as  $K_{ads}$ ,  $\Delta G_{ads}$ ,  $\Delta H_{ads}$ ,  $\Delta S_{ads}$  were calculated. The negative values of  $\Delta G_{ads}$ ,  $\Delta H_{ads}$  indicated a spontaneous exothermic adsorption process. The effect of temperature on the corrosion rate and the inhibition efficiency of LPD was examined using gravimetric measurements and the related activation parameters  $E_a$ ,  $\Delta S^*$ , and  $\Delta H^*$  of the corrosion process were also calculated. The surface analysis for MS morphology and composition after immersion in 1 M HCl for 24 h with and without addition of the optimum concentration of LPD was determined using AFM/SEM/EDX/FT-IR techniques. The following is the conclusion of the current study:

1. The investigated LPD is stable in 1 M HCl solution as their characteristic peak of imine group appeared unchanged in their UV-Visible spectra during different time intervals (1 h – 24 h).
2. The inhibition efficiencies of LPD increased as its concentration increased according to the obtained results from gravimetric, PDP, and EIS measurements.
3. The results of PDP describe the performance of LPD as a mixed – type inhibitor.
4. The adsorption of these LPD molecules acts in accordance with Langmuir model of adsorption at all temperatures.

5. The calculated values of  $\Delta G_{ads}$  refers to a combined physisorption and chemisorption mechanism.
6. The values of the calculated activation energy after addition of LPD was increased and so the corrosion rate decreased as compared with free acid solution.
7. The surface analysis using AFM/SEM/EDX/FT-IR techniques confirmed the corrosion inhibition behaviour of LPD and their adsorption on MS surface.

#### Declaration of Competing Interest

The authors declare that they have no known competing financial interests or personal relationships that could have appeared to influence the work reported in this paper.

#### Acknowledgements

The authors would like to express their gratitude to the Deanship of Graduate Studies (DGS) at Jouf University in Saudi Arabia for sponsoring and supporting this study through the DGS's Graduate Students Research Support (GSR) program. The authors also acknowledge that they used the central laboratory's facilities at Jouf University.

#### References

- [1] Callister, W. D.; Rethwisch, D. G. *Materials science and engineering: An introduction*. Wiley; New York. 2018. 9.
- [2] A. Umezokwere, I. Mbabuikwe, B. Oreko, D. Ezemuo, Corrosion rates and its impact on mild steel in some selected environments, *Journal of Scientific and Engineering Research* 3 (1) (2016) 34–43.
- [3] M.A. Ashraf, K. Mahmood, A. Wajid, M.J. Maah, I. Yusoff, Synthesis, characterization and biological activity of Schiff bases, *IPCBE* 10 (1) (2011) 185.
- [4] A.L. Berhanu, Gaurav, I. Mohiuddin, A.K. Malik, J.S. Aulakh, V. Kumar, K.-H. Kim, A review of the applications of Schiff bases as optical chemical sensors, *TrAC Trends in Analytical Chemistry* 116 (2019) 74–91.
- [5] H. Li, C. Dang, X. Tai, L. Xue, Y. Meng, S. Ma, J. Zhang, VALD-3, a Schiff base ligand synthesized from o-vanillin derivatives, induces cell cycle arrest and apoptosis in breast cancer cells by inhibiting the Wnt/ $\beta$ -catenin pathway, *Scientific reports* 11 (1) (2021) 1–14.
- [6] Q. Weng, J. Yi, X. Chen, D. Luo, Y. Wang, W. Sun, J. Kang, Z. Han, Controllable synthesis and biological application of schiff bases from D-glucosamine and terephthalaldehyde, *ACS omega* 5 (38) (2020) 24864–24870.
- [7] P. Dave, C. LV, Schiff based corrosion inhibitors for metals in acidic environment: A review, *Material Sci & Eng* 2 (6) (2018) 258–267.
- [8] R. Reeves, On the mechanism, substituent effects, and intramolecular catalysis in Schiff base hydrolysis, *The Journal of Organic Chemistry* 30 (9) (1965) 3129–3135.
- [9] R. Herscovitch, J. Charette, E. De Hoffmann, Physicochemical properties of Schiff bases. III. Substituent effects on the kinetics of hydrolysis of N-salicylidene-2-aminopropane derivatives, *Journal of the American Chemical Society* 96 (15) (1974) 4954–4958.
- [10] F. Lloret, M. Mollar, J. Faus, M. Julve, I. Castro, W. Diaz, Solution chemistry of N, N'-ethylenebis (salicylideneimine) and its copper (II), nickel (II) and iron (III) complexes, *Inorganica chimica acta* 189 (2) (1991) 195–206.

- [11] E. Barmatov, T. Hughes, Degradation of a schiff-base corrosion inhibitor by hydrolysis, and its effects on the inhibition efficiency for steel in hydrochloric acid, *Materials Chemistry and Physics* 257 (2021).
- [12] M. Prajila, A. Joseph, Inhibition of mild steel corrosion in hydrochloric using three different 1, 2, 4-triazole Schiff's bases: a comparative study of electrochemical, theoretical and spectroscopic results, *Journal of Molecular Liquids* 241 (2017) 1–8.
- [13] M. Murmu, S.K. Saha, N.C. Murmu, P. Banerjee, Effect of stereochemical conformation into the corrosion inhibitive behaviour of double azomethine based Schiff bases on mild steel surface in 1 mol L<sup>-1</sup> HCl medium: An experimental, density functional theory and molecular dynamics simulation study, *Corrosion Science* 146 (2019) 134–151.
- [14] M. Hosseini, S.F. Mertens, M. Ghorbani, M.R. Arshadi, Asymmetrical Schiff bases as inhibitors of mild steel corrosion in sulphuric acid media, *Materials Chemistry and Physics* 78 (3) (2003) 800–808.
- [15] L.A.M.E. Nassr, A.M. Abu-Dief, Kinetic Screening for the Acid-Catalyzed Hydrolysis of Some Hydrophobic Fe (II) Schiff Base Amino Acid Chelates and Reactivity Trends in the Presence of Alkali Halide and Surfactant, *International Journal of Chemical Kinetics* 47 (8) (2015) 501–508.
- [16] K.C. Emregül, O. Atakol, Corrosion inhibition of iron in 1 M HCl solution with Schiff base compounds and derivatives, *Materials Chemistry and Physics* 83 (2–3) (2004) 373–379.
- [17] A.B. Da Silva, E. D'Elia, J.A.d.C.P. Gomes, Carbon steel corrosion inhibition in hydrochloric acid solution using a reduced Schiff base of ethylenediamine, *Corrosion science* 52 (3) (2010) 788–793.
- [18] R. Gryboś, J. Szklarzewicz, A. Jurowska, M. Hodorowicz, Properties, structure and stability of V (IV) hydrazide Schiff base ligand complex, *Journal of Molecular Structure* 1171 (2018) 880–887.
- [19] W. Derafa, F. Paloukis, B. Mewafy, W. Baaziz, O. Ersen, C. Petit, G. Corbel, S. Zafeiratou, Synthesis and characterization of nickel-doped ceria nanoparticles with improved surface reducibility, *RSC Advances* 8 (2018) 40712–40719.
- [20] M.A. El-Hashemy, A. Sallam, The inhibitive action of *Calendula officinalis* flower heads extract for mild steel corrosion in 1 M HCl solution, *Journal of Materials Research and Technology* 9 (6) (2020) 13509–13523.
- [21] A. Fouda, H. Mostafa, G. Elewady, M. El-Hashemy, Low molecular weight straight-chain diamines as corrosion inhibitors for SS type 304 in HCl solution, *Chemical Engineering Communications* 195 (8) (2008) 934–947.
- [22] Hiromoto, S. 4 – Corrosion of metallic biomaterials. In *Metals for Biomedical Devices*, Niinomi, M., Ed. Woodhead Publishing. 2010. 99-121.
- [23] M.N. Uddin, D.A. Chowdhury, K. Hossain, Titanium(IV) Complexes of Unsymmetrical Schiff Bases Derived from Ethylenediamine and o-Hydroxyaldehyde/Ketone and Their Anti-microbial Evaluation, *Journal of The Chinese Chemical Society* 59 (2012) 1520–1527.
- [24] P.E. Aranha, M.P. dos Santos, S. Romera, E.R. Dockal, Synthesis, characterization, and spectroscopic studies of tetradentate Schiff base chromium (III) complexes, *Polyhedron* 26 (7) (2007) 1373–1382.
- [25] J. Liu, B.-W. Wu, B. Zhang, Y. Liu, Synthesis and characterization of metal complexes of Cu (II), Ni (II), Zn (II), Co (II), Mn (II) and Cd (II) with tetradentate Schiff bases, *Turkish Journal of Chemistry* 30 (1) (2006) 41–48.
- [26] N. Jha, D. Joshi, Synthesis and Configuration of Some Triorganoantimony (V) Chelates of Tetradentate Schiff Bases, Synthesis and Reactivity in Inorganic and Metal-Organic Chemistry 14 (4) (1984) 455–465.
- [27] P. Teyssie, J.J. Charette, Physico-chemical properties of coordinating compounds-III Infra-red spectra of N-salicyclidenealkylamines and their chelates, *Spectrochim. Acta* 19 (9) (1963) 1407–1423.
- [28] K. Ueno, A.E. Martell, Infrared Studies on Synthetic Oxygen Carriers, *The Journal of Physical Chemistry* 60 (9) (1956) 1270–1275.
- [29] M. Shakir, S. Hanif, M.F. Alam, H. Younus, Molecular hybridization approach of bio-potent CuII/ZnII complexes derived from N, O donor bidentate imine scaffolds: Synthesis, spectral, human serum albumin binding, antioxidant and antibacterial studies, *Journal of Photochemistry and Photobiology B: Biology* 165 (2016) 96–114.
- [30] S. Shit, G. Rosair, S. Mitra, A new tetranuclear copper (II) Schiff base complex containing Cu<sub>4</sub>O<sub>4</sub> cubane core: Structural and spectral characterizations, *Journal of Molecular Structure* 991 (1–3) (2011) 79–83.
- [31] C. Rimington, Spectral-absorption coefficients of some porphyrins in the Soret-band region, *Biochemical Journal* 75 (3) (1960) 620.
- [32] Felicio, R. C.; da Silva, G. A.; Ceridorio, L. F.; Dockal, E. R. Tetradentate Schiff base copper (II) complexes. *Synthesis and reactivity in inorganic and metal-organic chemistry*. 1999. 29 (2). 171-192.
- [33] A. Yurt, A. Balaban, S.U. Kandemir, G. Bereket, B. Erk, Investigation on some Schiff bases as HCl corrosion inhibitors for carbon steel, *Materials chemistry and physics* 85 (2–3) (2004) 420–426.
- [34] K. Ansari, M. Quraishi, Bis-Schiff bases of isatin as new and environmentally benign corrosion inhibitor for mild steel, *Journal of Industrial and Engineering Chemistry* 20 (5) (2014) 2819–2829.
- [35] K. Ansari, M. Quraishi, Experimental and quantum chemical evaluation of Schiff bases of isatin as a new and green corrosion inhibitors for mild steel in 20% H<sub>2</sub>SO<sub>4</sub>, *Journal of the Taiwan Institute of Chemical Engineers* 54 (2015) 145–154.
- [36] P. Dasami, K. Parameswari, S. Chitra, Corrosion inhibition of mild steel in 1M H<sub>2</sub>SO<sub>4</sub> by thiadiazole Schiff bases, *Measurement* 69 (2015) 195–201.
- [37] A.A. Farag, A.S. Ismail, M. Migahed, Environmental-friendly shrimp waste protein corrosion inhibitor for carbon steel in 1 M HCl solution, *Egyptian journal of petroleum* 27 (4) (2018) 1187–1194.
- [38] K. Hu, J. Zhuang, C. Zheng, Z. Ma, L. Yan, H. Gu, X. Zeng, J. Ding, Effect of novel cytosine-l-alanine derivative based corrosion inhibitor on steel surface in acidic solution, *Journal of Molecular Liquids* 222 (2016) 109–117.
- [39] M.H. Hussin, M.J. Kassim, Electrochemical, thermodynamic and adsorption studies of (+)-catechin hydrate as natural mild steel corrosion inhibitor in 1 M HCl, *International Journal of Electrochemical Science* 6 (5) (2011) 1396–1414.
- [40] P. Mourya, S. Banerjee, M. Singh, Corrosion inhibition of mild steel in acidic solution by *Tagetes erecta* (Marigold flower) extract as a green inhibitor, *Corrosion Science* 85 (2014) 352–363.
- [41] A.K. Singh, S. Mohapatra, B. Pani, Corrosion inhibition effect of Aloe Vera gel: Gravimetric and electrochemical study, *Journal of Industrial and Engineering Chemistry* 33 (2016) 288–297.
- [42] Wisdom O, J. Adsorption and Corrosion inhibition of *Gnetum africanum* leaves extract on carbon steel. *International journal of materials and chemistry*. 2013. 3. 10-16.
- [43] H.M. Elaryian, M.A. Bedair, A.H. Bedair, R.M. Aboushahba, A.-A. Fouda, Synthesis, characterization of novel coumarin dyes as corrosion inhibitors for mild steel in acidic environment: Experimental, theoretical, and biological studies, *Journal of Molecular Liquids* 346 (2022).
- [44] P. Atkins, J. de Paula, *Elements of Physical Chemistry*, OUP Oxford (2013).



- [45] Laidler, K. J.; Meiser, J. H.; Sanctuary, B. C. *Physical Chemistry*. Houghton Mifflin. 2002.
- [46] S. Shahabi, S. Hamidi, J.B. Ghasemi, P. Norouzi, A. Shakeri, Synthesis, experimental, quantum chemical and molecular dynamics study of carbon steel corrosion inhibition effect of two Schiff bases in HCl solution, *Journal of Molecular Liquids* 285 (2019) 626–639.
- [47] MOHD N k, CORROSION INHIBITION OF MILD STEEL IN HYDROCHLORIC ACID SOLUTION USING FATTY ACID DERIVATIVES, *Journal of Oil Palm Research* 29 (1) (2017) 97–109.
- [48] S. Li, H. Ma, S. Lei, R. Yu, S. Chen, D. Liu, Inhibition of copper corrosion with Schiff base derived from 3-methoxysalicylaldehyde and O-phenyldiamine in chloride media, *Corrosion* 54 (12) (1998) 947–954.
- [49] N. Maghraoui, D. Aggoun, B. Bouzerafa, H. Bezzi, Y. Ouennoughi, D. López, M. Fernández García, A. Ourari, M. S. Mubarak, Synthesis, characterization, thermal stability, electrochemical behavior, and antioxidant activity of new oxovanadium(iv) and iron(ii) tetradentate Schiff base complexes, *Arabian Journal of Chemistry* 14 (3) (2021).
- [50] H.H. Hassan, E. Abdelghani, M.A. Amin, Inhibition of mild steel corrosion in hydrochloric acid solution by triazole derivatives: Part I, Polarization and EIS studies. *Electrochimica Acta* 52 (22) (2007) 6359–6366.
- [51] P.R. Ammal, M. Prajila, A. Joseph, Physicochemical studies on the inhibitive properties of a 1, 2, 4-triazole Schiff's base, HMATD, on the corrosion of mild steel in hydrochloric acid, *Egyptian Journal of Petroleum* 27 (3) (2018) 307–317.